^{18}F-fluorodeoxyglucose Positron Emission Tomography in Kaposi Sarcoma Herpesvirus–Associated Multicentric Castleman Disease: Correlation With Activity, Severity, Inflammatory and Virologic Parameters

Mark N. Polizzotto,[1] Corina Millo,[3] Thomas S. Uldrick,[1] Karen Aleman,[1] Millie Whatley,[3] Kathleen M. Wyvill,[1] Deirdre O'Mahony,[1] Vickie Marshall,[4] Denise Whitby,[4] Roberto Maass-Moreno,[3] Seth M. Steinberg,[2] Richard F. Little,[1] and Robert Yarchoan[1]

[1]HIV and AIDS Malignancy Branch, [2]Biostatistics and Data Management Section, Center for Cancer Research, National Cancer Institute, [3]Positron Emission Tomography Department, Warren G. Magnuson Clinical Center, National Institutes of Health, Bethesda, and [4]Viral Oncology Section, AIDS and Cancer Virus Program, Frederick National Cancer Laboratory for Cancer Research, Maryland

Background. Kaposi sarcoma herpesvirus (KSHV)-associated multicentric Castleman disease (MCD) is a lymphoproliferative inflammatory disorder commonly associated with human immunodeficiency virus (HIV). Its presentation may be difficult to distinguish from HIV and its complications, including lymphoma. Novel imaging strategies could address these problems.

Methods. We prospectively characterized ^{18}F-fluorodeoxyglucose positron emission tomography (PET) findings in 27 patients with KSHV-MCD. Patients were imaged with disease activity and at remission with scans evaluated blind to clinical status. Symptoms, C-reactive protein level, and HIV and KSHV loads were assessed in relation to imaging findings.

Results. KSHV-MCD activity was associated with hypermetabolic symmetric lymphadenopathy (median maximal standardized uptake value [SUV_{max}], 6.0; range, 2.0–8.0) and splenomegaly (3.4; 1.2–11.0), with increased metabolism also noted in the marrow (2.1; range, 1.0–3.5) and salivary glands (3.0; range, 2.0–6.0). The ^{18}F-fluorodeoxyglucose PET abnormalities improved at remission, with significant SUV_{max} decreases in the lymph nodes ($P = .004$), spleen ($P = .008$), marrow ($P = .004$), and salivary glands ($P = .004$). Nodal SUV_{max} correlated with symptom severity ($P = .005$), C-reactive protein level ($R = 0.62$; $P = .004$), and KSHV load ($R = 0.54$; $P = .02$) but not HIV load ($P = .52$).

Conclusions. KSHV-MCD activity is associated with ^{18}F-FDG PET abnormalities of the lymph nodes, spleen, marrow, and salivary glands. These findings have clinical implications for the diagnosis and monitoring of KSHV-MCD and shed light on its pathobiologic mechanism.

Keywords. Castleman disease; human herpesvirus 8 (HHV-8)/Kaposi sarcoma herpesvirus (KSHV); HIV; ^{18}F-FDG positron emission tomography.

Kaposi sarcoma (KS) herpesvirus (KSHV)–associated multicentric Castleman disease (MCD) is a lymphoproliferative inflammatory disorder most common in persons with human immunodeficiency virus (HIV) [1–8]. Its manifestations include fever, cytopenias, and hypoalbuminemia [1–4]. Clinical activity is associated with elevations in KSHV viral load and levels of C-reactive protein (CRP), KSHV-encoded viral interleukin 6 (vIL-6), and/or human interleukin 6 (hIL-6) [9–11]. Many cases arise in patients with suppressed HIV loads and preserved CD4 cell counts [12–14]. Patients commonly exhibit other KSHV-associated tumors, including KS and primary effusion lymphoma (PEL) and are at high risk of developing large-cell lymphoma [15–17].

Diagnosis and monitoring of KSHV-MCD presents unique challenges. Its symptoms are intermittent and difficult to distinguish from HIV, opportunistic infection, and concurrent lymphoma [3, 4]. Distinction of these carries major therapeutic and prognostic implications and generally rests on histopathologic findings, but "blind" selection of a lymph node for biopsy may not capture the spectrum of disease present. Assessment of response to therapy is also challenging. Current response criteria are variable and generally do not include imaging [3, 12–14]. The optimal end point of therapy and relapse surveillance strategy remain undefined [3–5, 12–14].

[18]F-fluorodeoxyglucose (^{18}F-FDG) positron emission tomography (PET) provides a potentially useful technique to assess KSHV-MCD. It has established utility in the management of lymphomas, including HIV-associated lymphomas [18–24]. In large-cell lymphoma, involved sites are characterized by markedly increased ^{18}F-FDG uptake [18, 19]. In uncontrolled HIV infection, moderate generalized increases in uptake are seen in lymph nodes but not other tissues [20, 25–29], and patients in whom HIV viral load is suppressed by antiretroviral therapy do not exhibit ^{18}F-FDG PET abnormalities [25, 27]. The use of ^{18}F-FDG PET has also been proposed for imaging other inflammatory and infective states [30–34]. There has been little assessment of ^{18}F-FDG PET in KSHV-MCD. The existing studies are small retrospective series evaluating limited anatomic sites, that have not followed subjects to remission or evaluated ^{18}F-FDG PET in relation to correlates of disease activity [35–38].

We undertook a prospective study whose primary objective was to determine whether ^{18}F-FDG PET abnormalities were identifiable in active KSHV-MCD compared with remission. We also considered whether ^{18}F-FDG PET could help distinguish KSHV-MCD from comorbid conditions and assist in biopsy site selection, and we explored the relationship of ^{18}F-FDG PET abnormalities to symptom severity, correlates of activity disease (including CRP and KSHV load), and HIV replication.

METHODS

Population

Patients with histopathologically confirmed KSHV-MCD were enrolled in a natural history protocol (NCT00099073) incorporating investigational therapies including zidovudine with valganciclovir [12], and rituximab with liposomal doxorubicin [39]. Evaluation of ^{18}F-FDG PET was a prospectively specified objective. According to the protocol, ^{18}F-FDG PET with computed tomography (CT) was performed when patients developed KSHV-MCD activity, except when they were too clinically unstable, and also after remission. The protocol was approved by the National Cancer Institute (NCI) Institutional Review Board. All patients gave written informed consent.

Clinical Assessment

Disease severity was graded using NCI Common Toxicity Criteria for Adverse Events (CTCAE), version 3.0 [40]. Symptomatic disease activity was defined as the presence of ≥1 symptom and ≥1 laboratory abnormality attributable to KSHV-MCD [12]. For this analysis, to ensure the broadest spectrum of disease was captured, we included patients with laboratory abnormalities attributable to KSHV-MCD but no symptoms. Remission was evaluated using NCI-HIV and AIDS Malignancy Branch clinical criteria [12]. Patients were evaluated clinically once per cycle of therapy (usually 3 weeks) while being treated for KSHV-MCD and then every 3 months.

Functional Imaging

Patients received a median ^{18}F-FDG dose of 15.5 mCi (range, 11.5–16.4 mCi) intravenously after fasting for ≥6 hours; the median glucose level was 96 mg/dL (range, 73–192 mg/dL). Images were acquired from the base of skull to the middle of the thigh, starting a mean (standard deviation) of 60 ± 5 minutes after injection, using a GE Discovery ST PET/CT scanner (General Electric Healthcare), except early in the study when 8 ^{18}F-FDG PET–only studies were performed using a GE Advance scanner. After an equipment upgrade, 1 scan was performed using a Siemens Biograph 64 PET/CT scanner (Siemens AG) For PET/CT scans, CT was performed at 35 mA (GE Discovery) or 34 mA (Siemens) and 120 kV.

Imaging Assessment

Analysis was performed blinded to clinical information using MedView (MedImage). Sites with activity increased above physiologic baseline were considered abnormal and graded based on visual intensity in comparison to the mediastinal blood pool. Quantitative analysis was performed by determining the standardized uptake value (SUV; [voxel activity-concentration] × [patient weight/injected activity]). Regions of interest were drawn over the liver, spleen, visualized nodes, L5 marrow, salivary glands, tonsils, testes, and any other abnormal areas to determine organ-specific maximal SUV (SUV_{max}). Where nodes were not discernible, they were assigned an SUV equivalent to background. As imaged lymph nodes were commonly small and changed in size from active disease to remission, partial volume correction (PVC) to correct for known effects of lesion size on derived SUV, particularly in smaller lesions, was performed for nodal SUV_{max}, using measured target nodal size and a recovery coefficient derived for each scanner and calculation methods described elsewhere [41]. Nodal PVC SUV_{max} is reported separately. Other organs of interest were large and relatively stable in size so PVC was not performed for those SUVs.

Laboratory Assays

KSHV viral load in peripheral blood mononuclear cells was assessed with quantitative real-time polymerase chain reaction, as described elsewhere [9]. CRP levels were assayed using the

Siemens Dimension Vista platform (Siemens AG). A standard sensitivity assay was used until May 2009 and then replaced by a high sensitivity assay; values were harmonized as described elsewhere [12]. CD4 T-lymphocyte counts were assessed by means of fluorescent-activated cell sorting using the BlueOcean platform (Beckman Coulter). Plasma HIV-1 RNA levels were measured with quantitative polymerase chain reaction, using the Roche Amplicor assay (Roche Diagnostic Systems).

Statistical Analysis

Paired analyses of organ-specific SUV_{max} and, for nodes, PVC SUV_{max} at disease activity and remission were performed using the Wilcoxon signed rank test. Associations between SUV_{max} and disease parameters were explored using Spearman correlations for continuous variables, CRP, and log_{10}(KSHV load); Jonckheere–Terpstra test for trend in ordered categorical variables from independent samples for symptom grade; and exact Wilcoxon rank sum test for HIV load, categorized as undetectable or detectable (≤ 50 or > 50 copies/mL plasma, respectively).

RESULTS

Patients

A total of 27 patients underwent imaging. Of these, 3 patients had lymphoma in addition to KSHV-MCD; these were excluded from the primary analysis and are discussed separately below. For the remaining 24 patients, the median age was 43 years (range, 34–56 years); 22 patients (92%) were male, and all were HIV infected and receiving antiretroviral therapy (Table 1). Nineteen patients underwent scanning while they had active KSHV-MCD: 16 had symptomatic disease ("flares"), and 3 had laboratory manifestations. Of these 19 patients, 16 were also scanned during remission and had paired comparisons; the remaining 3 did not achieve remission. Five patients were studied only during remission: 2 were critically ill during flares and could not be imaged, and 3 did not manifest active disease. Thus, 21 patients underwent scanning during remission. HIV control was similar across each time point (median HIV viral load undetectable at both), with modest differences in CD4 cell counts. The median follow-up time in the study was 79 weeks (range, 8–293 weeks), and for patients with paired scans, the median time between scans at active disease and remission was 80 weeks (range, 8–233 weeks).

Imaging Findings and Disease Activity

All ^{18}F-FDG PET scans performed during active disease showed metabolic abnormalities (Table 2; representative example in Figure 1). The most common and marked abnormalities were in the lymph nodes and spleen. During remission, 11 scans (53%) showed no metabolic or anatomic abnormality at any site (Figure 1). The remaining 10 (47%) exhibited minor nodal abnormalities, and 2 also had minor splenic abnormalities.

Table 1. Patient Characteristics During KSHV-MCD Activity and Remission[a]

Characteristic	Active Disease (n = 19)	Remission (n = 21)[b]
Symptomatic disease, No. (%)	16 (84)	0
Symptoms present, No.[c]	4 (0–10)	0
CTCAE grade for most severe symptom[d]	2 (0–4)	NA
ECOG performance status	1 (0–2)	0 (0–1)
Temperature, °C	36.8 (35.9–39.5)	36.3 (35.3–37.2)
Hemoglobin, g/dL	10.1 (8.0–14.4)	12.9 (10.3–15.0)
Platelet count, 10^3 cells/μL	155 (25–567)	201 (118–438)
Leukocyte count, 10^3 cells/μL	5.3 (1.0–15.7)	4.4 (1.8–10.9)
Sodium, mmol/L	136 (126–139)	137 (135–142)
Albumin, g/dL	2.8 (1.7–4.0)	4.1 (3.5–4.5)
C-reactive protein, g/dL	16 (0.7–211)	3.8 (<0.3–14.0)
KSHV viral load, copies/10^6 PBMCs	4545 (0–585 714)	0 (0–2848)
Receiving ART, No. (%)	19 (100)	21 (100)
HIV viral load, copies/mL	<50 (<50–7710)	<50 (<50–2781)
HIV viral load undetectable (<50 copies/mL), No. (%)	13 (68)	19 (90)
CD4 cell count, cells/μL	286 (67–1319)	380 (139–841)

Abbreviations: ART, antiretroviral therapy; CTCAE, National Cancer Institute Common Toxicity Criteria for Adverse Events; ECOG, Eastern Cooperative Oncology Group; HIV, human immunodeficiency virus; KSHV, Kaposi sarcoma herpesvirus; KSHV-MCD, KSHV-associated multicentric Castleman disease; NA, not applicable; PBMCs, peripheral blood mononuclear cells.

[a] Unless otherwise noted, values represent medians (ranges).

[b] Any abnormalities noted during remission were not attributable to KSHV-MCD.

[c] All clinical symptoms attributable to KSHV-MCD, including fever but not laboratory abnormalities.

[d] Most severe symptom attributable to KSHV-MCD.

Lymph Node Findings

The most common abnormality during disease activity was symmetric hypermetabolic lymphadenopathy, present in all patients. This was most marked in the axilla, neck, and mediastinum. In 15 patients (79%), there were widespread abnormalities; in 4 (21%), abnormalities were restricted (to the mediastinum in 2, the mediastinum and axillae in 1, and the inguinal and supraclavicular regions in 1). Nodal metabolic abnormalities were graded as moderate or marked in 12 patients (63%) and mild in 7 (37%). The median nodal SUV_{max} for all subjects was 6.0 (range, 2.0–8.0); with PVC, the median SUV_{max} was 6.5 (range, 2.0–8.9).

Patients with symptomatic active disease exhibited more marked nodal changes than those with only laboratory abnormalities: 15 (94%) showed diffuse hypermetabolic lymphadenopathy, moderate or marked in 12 (75%), with a median

Table 2. ^{18}F-FDG PET/CT Findings During KSHV-MCD Activity and Remission

^{18}F-FDG PET/CT Abnormality	Active KSHV-MCD (n = 19)			Remission (n = 21)		
	Any Abnormality, No. (%)	Moderate or Marked Abnormality, No. (%)	SUV$_{max}$, Median (Range)	Any Abnormality No. (%)	Moderate or Marked Abnormality No. (%)	SUV$_{max}$, Median (Range)
Lymph nodes						
Any	19 (100)	12 (63)	6.0 (2.0–8.0)	10 (48)	1 (5)	2.0 (1.0–7.1)
Diffuse	15 (79)	NA	NA	4 (19)	NA	NA
Focal	4 (21)	NA	NA	6[a] (29)	NA	NA
Spleen[b]						
Any	16 (89)	4 (22)	3.4 (1.2–11.0)	2 (10)	0	1.9 (1.5–4.2)
Metabolic	14 (78)	NA	NA	2 (10)	0	NA
Anatomic	14 (78)	NA	NA	0	0	NA
Liver						
Any	4 (21)	0	2.3 (2.0–3.2)	0	0	2.0 (1.8–4.2)
Metabolic	0	NA	NA	0	0	NA
Anatomic	4 (21)	NA	NA	0		NA
Bone marrow	11 (58)	0	2.1 (1.0–3.5)	2[c] (10)	0	1.2 (1.0–4.2)
Tonsils	5 (26)	4 (21)	2.6 (2.2–10.3)	6 (29)	1 (5)	3.0 (2.1–10.0)
Salivary glands	6 (32)	0	3.0 (2.0–6.0)	3 (14)	0	3.0 (2.0–6.4)
Testes[d]	0	0	3.2 (2.0–4.5)	0	0	3.5 (2.0–4.6)

Abbreviations: ^{18}F-FDG, ^{18}F-fluorodeoxyglucose; CT, computed tomography; KSHV-MCD, Kaposi sarcoma herpesvirus–associated multicentric Castleman disease; NA, not applicable; PET, positron emission tomography; SUV$_{max}$, maximal standardized uptake value.

[a] Two focal nodes were adjacent to intercurrent disease (infection and avascular necrosis in 1 patient each).

[b] Of 18 patients with intact spleens at active disease and 20 at remission.

[c] One after granulocyte colony-stimulating factor treatment and 1 diagnosed with chronic myeloid leukemia 3 months later.

[d] Of 16 male patients at active disease (1 scan in a male patient omitted the testes) and 19 male at remission.

nodal SUV$_{max}$ of 6.2 (range, 2.0–8.0) and a median PVC nodal SUV$_{max}$ of 6.6 (range, 2.0–8.9). All patients with severe symptoms (NCI CTCAE grade ≥3) demonstrated moderate or severe diffuse adenopathy. In contrast, the 3 with asymptomatic activity had mild, restricted abnormalities (median SUV$_{max}$, 2.0; range. 2.0–5.2; median PVC SUV$_{max}$, 2.2; range, 2.0–5.2).

At remission, nodal abnormalities were present in 10 patients (47%); these were diffuse in 4 (19%) and focal in 6 (27%). The nodal abnormalities were graded as mild in 9 patients and moderate in 1. The median nodal SUV$_{max}$ at remission was 2.0 (range, 1.0–7.1). Two patients with focal nodal abnormalities had intercurrent disease that may have explained the changes (soft-tissue infection and adjacent avascular necrosis in 1 patient each). Among the 16 paired patients, the nodal SUV$_{max}$ decreased during remission in 14 (88%); in the 2 for whom it did not, 1 reported local inflammation after injury, and the other had no apparent explanation (neither were HIV viremic). In these paired studies, nodal SUV$_{max}$ was significantly lower at remission, with and without PVC (median absolute decrease in SUV$_{max}$ 2.4 [$P = .004$]; median absolute decrease in PVC SUV$_{max}$ 2.1 [$P = .004$]; see Figure 2).

Splenic Findings

Increased splenic metabolic activity and splenomegaly were common in the 18 patients with intact spleens; overall, 16 patients (89%) had splenic abnormalities. Metabolic activity was diffusely increased in 14 patients (78%); this was graded as moderate or severe in 4 (22%). Fourteen patients (78%) had splenomegaly. Two patients had splenic hypermetabolism without splenomegaly, and 2 had splenomegaly without increased in metabolism. The median splenic SUV$_{max}$ for all subjects was 3.4 (range, 1.2–11.0). Splenic abnormalities were more marked in symptomatic patients. Of 15 patients with symptomatic flares and intact spleens, ^{18}F-FDG PET showed increased metabolic activity in 13 (87%), moderate or severe in 4 (27%). The median splenic SUV$_{max}$ in symptomatic patients was 3.7 (range, 1.5–4.8). Of 3 patients with only laboratory evidence of disease activity, 2 had splenic abnormalities: 1 (with concurrent toxoplasmosis and tuberculosis) had increased splenic metabolic activity with splenomegaly, and 1 had splenomegaly alone (median SUV$_{max}$, 1.5; range, 1.2–11.0).

Of 20 patients with intact spleens at remission, 2 (10%) had mild splenic metabolism without splenomegaly; both also had nodal abnormalities. Median splenic SUV$_{max}$ at remission was
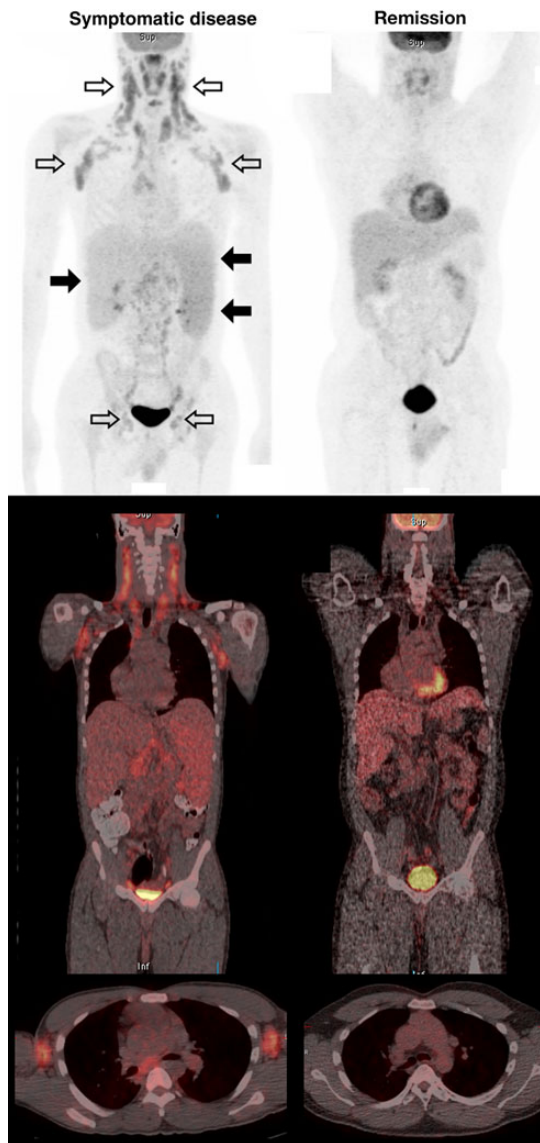
Figure 1. Representative ^{18}F-fluorodeoxyglucose positron emission tomographic (PET)/computed tomographic (CT) studies during Kaposi sarcoma herpesvirus–associated multicentric Castleman disease (KSHV-MCD) activity and remission. *Top,* Representative images (maximum intensity projection. *Middle and bottom,* PET/CT composites from a single patient with active symptomatic disease (*left*) and later during remission (*right*). The diagnosis of KSHV-MCD was confirmed by excisional biopsy of a right inguinal lymph node. At both time points, the human immunodeficiency virus load was undetectable (<50 copies/mL); the CD4 cell count was 295 cells/µL during active disease and 238 cells/µL at remission. The scan obtained during KSHV-MCD activity shows diffuse hypermetabolic lymphadenopathy, most marked in the neck and axillae but also involving pelvic and inguinal nodes (*open arrows*), splenomegaly with increased metabolism (*closed arrows on right*), hepatomegaly without any increase in metabolism (*closed arrows on left*), and generalized increased marrow metabolism. The anatomic correlation of these abnormalities with the nodes and organs is illustrated in the PET/CT composites (*middle and bottom panels*), including a horizontal section showing axillary nodal uptake (*bottom panel*). These abnormalities are each seen to have resolved in the scan obtained at remission. The remission scan shows normal cardiac activity, and both scans show normal tracer accumulation in the bladder.

1.9 (range, 1.5–4.2). Of 15 paired studies in patients with intact spleens, the splenic SUV_{max} decreased in 14 (93%). The median absolute decrease in splenic SUV_{max} was 1.8 ($P = .009$).

Bone Marrow Findings

Mild increases in marrow metabolic activity were present in 11 patients (58%); all had symptomatic disease. The median marrow SUV_{max} at active disease was 2.15 (range, 1.0–3.5). In 2 patients, increases in marrow metabolic activity persisted at remission. Alternate explanations were likely in both patients: 1 had received granulocyte stimulating factor, and 1 had developed chronic myeloid leukemia. The median marrow SUV_{max} at remission was 1.2 (1.0–4.2); in paired patients, the median marrow SUV_{max} was significantly lower at remission (median absolute decrease, 0.8; $P = .004$).

Salivary and Tonsillar Findings

Six patients (32%) exhibited a symmetric increase in salivary gland metabolism during activity (all mild); the median salivary SUV_{max} was 3.0 (2.0–6.0). In 3 patients, this persisted at remission (all mild); the median salivary SUV_{max} at remission was 3.0 (range, 2.0–6.4). In the 16 paired patients, the median salivary SUV_{max} was significantly lower at remission (median absolute decrease, 0.8; $P = .004$).

Five patients (26%) had increases in tonsillar uptake during disease activity. The median tonsillar SUV_{max} at activity was 2.6 (2.2–10.3). Six (29%) patients had tonsillar hypermetabolism at remission (mild in 5), and the median tonsillar SUV_{max} at remission remained elevated at 3.0 (2.1–10.0), with no change in tonsillar SUV_{max} between active disease and remission (median absolute decrease, 0.05; $P = .96$).

Hepatic Findings

At active disease 4 patients (21%), all symptomatic, had hepatomegaly without any change in hepatic metabolism (median SUV_{max} 2.3; range, 2.0–3.2). None had hepatomegaly or increased hepatic metabolism at remission (median SUV_{max}, 2.0; range, 1.8–4.2), and there was no significant change in hepatic SUV_{max} in paired studies (median absolute in decrease SUV_{max}, 0.2; $P = .59$).

Findings at Other Sites

In 2 patients, pleural effusions (not ^{18}F-FDG avid) were noted during active disease; neither patient was found to have PEL. In 1 patient, several PET-avid cystic bone lesion of the axial skeleton were present (SUV_{max} 4.4). Multiple moderately avid pulmonary lesions were also noted in the patient with toxoplasmosis and tuberculosis, persisting at KSHV-MCD remission. All male patients had normal testicular metabolic activity (Table 1), with no change in testicular SUV_{max} between active disease and remission (median decrease in SUV_{max} 0.0; $P = .80$).
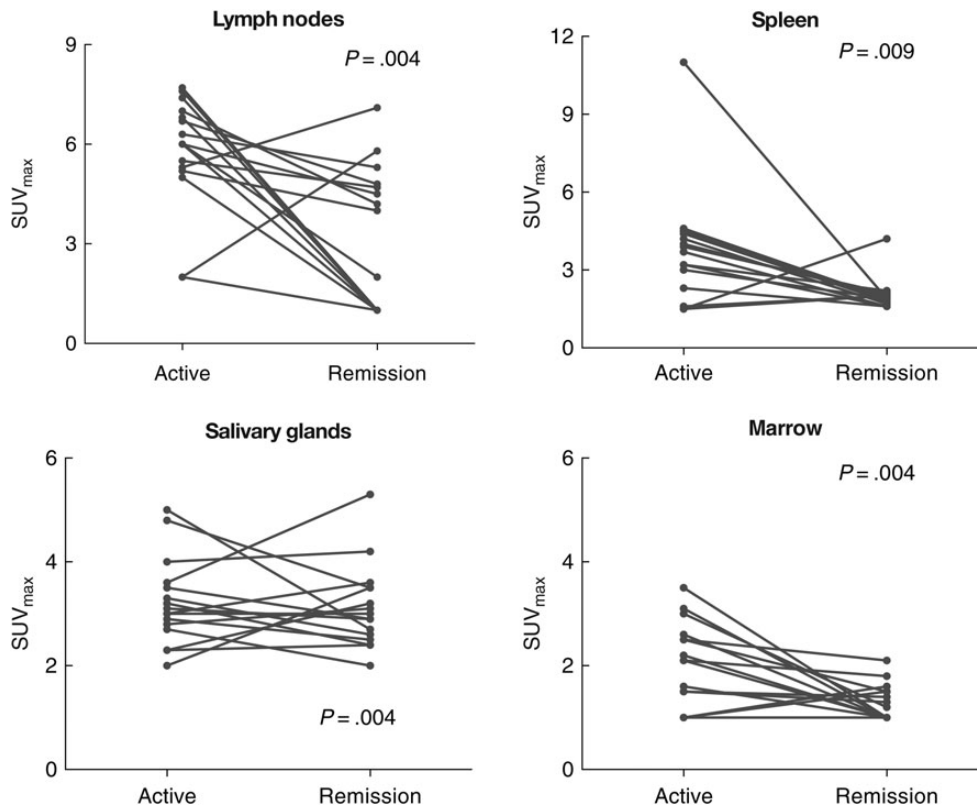
Figure 2. Individual subject changes in overall and organ-specific quantitative ^{18}F-fluorodeoxyglucose positron emission tomographic (PET) abnormalities between flare and remission. Comparison of organ-specific maximal standardized uptake value (SUV_{max}) between active disease and remission in patients with paired PET scans (n = 16 but n = 15 for spleen) showed statistically significant reductions in metabolic activity of lymph nodes, spleen, salivary glands, and bone marrow; changes were most marked for nodes and spleen. For lymph nodes, this difference remained significant with partial volume correction (PVC) (median decrease in PVC SUV_{max}, 2.1; $P = .004$ [not shown]). Note that the vertical axis scales differ.

Imaging Association with Disease Severity and Correlates of Disease Activity

We used nodal SUV_{max} to explore the relationship of ^{18}F-FDG PET with disease severity in subjects with active disease, because nodal abnormalities were the most common and dynamic indicator of disease. We used CRP level and KSHV load as laboratory markers of severity, because these are well correlated with activity and with serum levels of vIL-6 and hIL-6 [9], and we explored any relationship with HIV viremia. KSHV-MCD symptom severity during disease activity was associated with the intensity of nodal abnormalities as assessed by nodal SUV_{max} with and without PVC ($P = .004$ by Jonckheere–Terpstra trend test; with PVC, $P = .013$; Figure 3). Nodal SUV_{max} was also correlated with both CRP level ($R = 0.62$; $P = .004$) and KSHV viral load ($R = 0.54$; $P = .02$) (Figure 3); these correlations were also present after PVC (for CRP and PVC nodal SUV_{max} $R = 0.55$ and $P = .01$; for KSHV viral load and PVC nodal SUV_{max}, $R = 0.46$ and $P = .05$). By contrast, there was no association between nodal SUV_{max} with or without PVC and HIV viral load ($P = .52$ for nodal SUV_{max} and $P = .92$ for PVC nodal SUV_{max}).

Imaging Before Symptomatic Relapse

Three ^{18}F-FDG PET/CT scans had been obtained at an outside center in a patient who had achieved KSHV-MCD remission before experiencing a symptomatic relapse and enrolling in the present study (SUV could not be calculated, and these scans are not included in the primary analyses). The scans demonstrated progressive abnormalities before relapse with increasing splenic metabolic activity and size and the development of widespread hypermetabolic adenopathy (Figure 4). One month after the final scan, this patient experienced a symptomatic relapse for which he was treated, after which ^{18}F-FDG PET abnormalities resolved.

Imaging of Intercurrent Tumors

Intercurrent lymphomas were identified in 3 patients: 2 had KSHV-associated PEL, and 1 had diffuse large B-cell lymphoma. None had symptoms attributable to KSHV-MCD at imaging. Each had ^{18}F-FDG PET abnormalities distinguishable from KSHV-MCD by their avidity and distribution (Figure 5), with intensely hypermetabolic abnormalities restricted to sites of
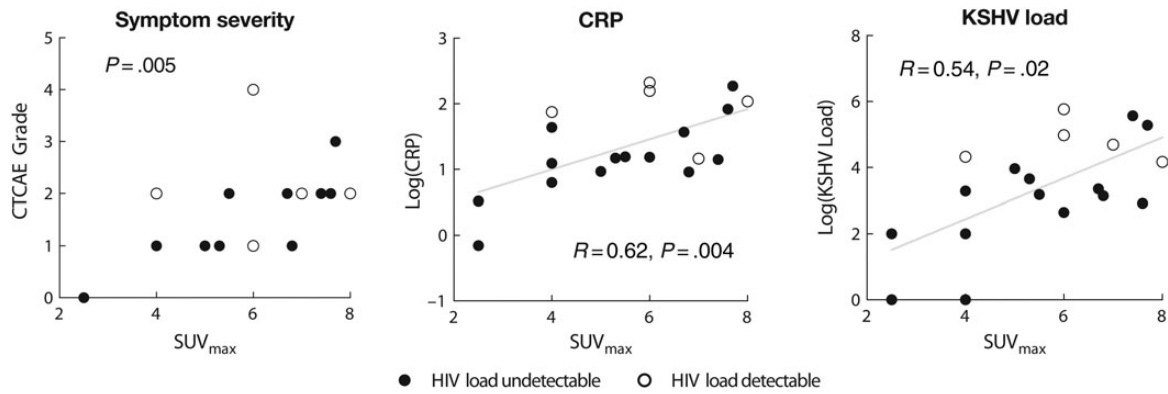
Figure 3. Association of quantitative intensity of ^{18}F-fluorodeoxyglucose positron emission tomographic abnormalities with Kaposi sarcoma herpesvirus–associated multicentric Castleman disease (KSHV-MCD) disease parameters. In patients with active KSHV-MCD, nodal maximal standardized uptake value (SUV$_{max}$) was correlated with symptom grade (National Cancer Institute Common Toxicity Criteria for Adverse Events [CTCAE] grade for worst symptom present; $P = .005$ by Jonckheere–Terpstra test for trend) and moderately well correlated with 2 established laboratory indicators of KSHV-MCD disease activity, C-reactive protein (CRP) ($R = 0.62$ and $P = .004$; regression line shown) and KSHV load ($R = 0.54$ and $P = .02$; regression line shown). Abbreviation: HIV, human immunodeficiency virus.

lymphoma involvement. Otherwise, these patients had normal uptake. The median SUV$_{max}$ at sites involved with lymphoma was 11.0 (range 7.0–38.2).

Nine patients had cutaneous KS within the imaged field. (Others had active KS in extremities outside the field.) Mildly hypermetabolic cutaneous abnormalities were visualized at involved sites in 5 (55%) (Figure 5); the median SUV of these lesions was 3.0 (range, 2.0–4.0). In 1 patient whose KS remitted between the initial and remission studies, the cutaneous hypermetabolic abnormalities resolved.
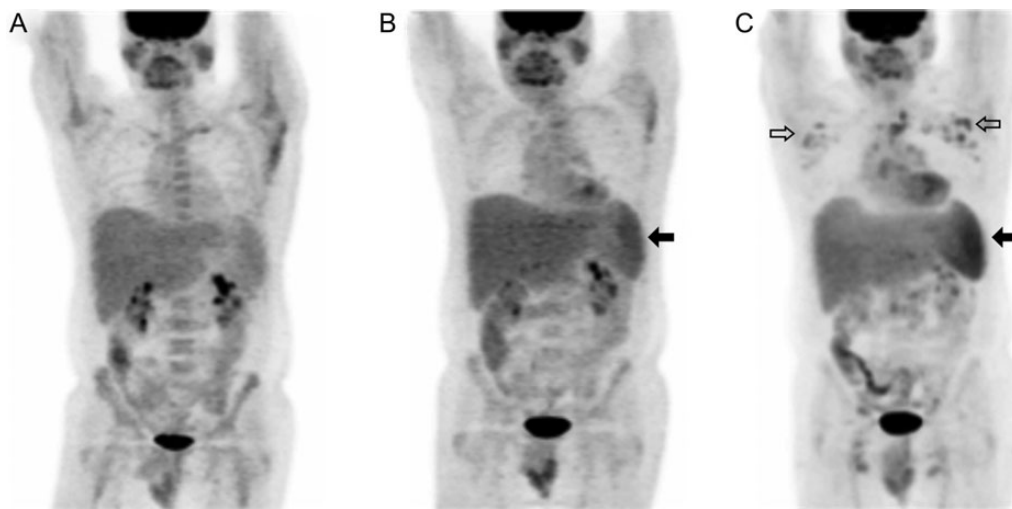

Figure 4. Progressive ^{18}F-fluorodeoxyglucose (^{18}F-FDG) positron emission tomographic (PET) abnormalities preceding symptomatic relapse of Kaposi sarcoma herpesvirus–associated multicentric Castleman disease (KSHV-MCD). Panels show sequential ^{18}F-FDG PET scans performed in a single patient at time points after the first remission of symptomatic KSHV-MCD. Maximum intensity projections are shown. *A*, At first remission, the only metabolic abnormality was a mild increase in isolated axillary nodes. *B*, Four months into remission, while the patient was still clinically asymptomatic, splenic metabolism was mild with was borderline splenomegaly (*closed arrow*); nodal abnormalities were slightly more prominent. *C*, Ten months into remission, while the patient was still asymptomatic, splenic metabolism was markedly increased with persisting borderline splenomegaly (*closed arrow*), and moderately hypermetabolic adenopathy was seen, most marked in the axillary nodes but also involving cervical and inguinal sites (*open arrows*). Two months later, the patient experienced a symptomatic relapse and was enrolled in the present study and treated. These abnormalities resolved completely with his second remission (not shown).
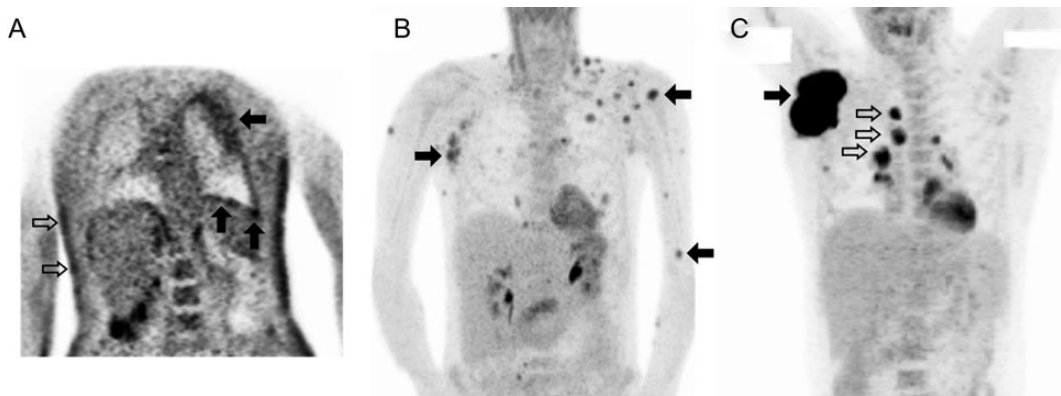
Figure 5. Findings of ^{18}F-fluorodeoxyglucose (^{18}F-FDG) positron emission tomography (PET) in patients with intercurrent tumors, including primary effusion lymphoma (PEL), diffuse large B-cell lymphoma, and Kaposi sarcoma (KS). Representative ^{18}F-FDG PET maximum intensity projections from 3 patients with KS herpesvirus–associated multicentric Castleman disease (KSHV-MCD) and intercurrent tumors, including large-cell lymphomas and KS. *A,* In a patient with KSHV-MCD and PEL of both pleural cavities and severe cutaneous KS, the pleural surface demonstrates moderately increased avidity throughout, with patches of intense uptake (*closed arrows;* pleural nodal maximal standardized uptake value [SUV$_{max}$, 7.0]), whereas the lymphomatous effusion (*above lower closed arrows*) is not ^{18}F-FDG avid. Areas of moderate hypermetabolic activity are also seen in the skin at sites of KS involvement (*open arrows*). Lymph nodes and spleen were metabolically normal. The acquired imaging field and image quality in this patient was reduced owing to his critical illness. *B,* In a patient with KSHV-MCD and extracavitary PEL presenting with cutaneous and soft tissue, marked areas of avidity are seen at the sites of extracavitary PEL (*closed arrows;* lesion SUV$_{max}$, 11.0), while nodes are normal; the patient had previously undergone a splenectomy. *C,* In a patient with KSHV-MCD and diffuse large B-cell lymphoma, intense avidity is seen at the primary lymphomatous mass (*closed arrow;* SUV$_{max}$, 38.2) and less intense avidity at nearby involved nodes (*open arrows*), whereas uninvolved nodes and spleen are normal. Normal cardiac uptake is seen in *B* and *C,* and normal tracer excretion into the renal collecting system in *B.*

DISCUSSION

This prospective exploration of ^{18}F-FDG PET in KSHV-MCD characterizes imaging abnormalities during disease activity and remission, providing paired observations in individual patients and correlation of imaging findings with clinical and laboratory correlates of disease severity. Our findings suggest that ^{18}F-FDG PET can provide important information in patients with suspected KSHV-MCD, assist the distinction between KSHV-MCD and HIV and concurrent diseases, and shed light on its underlying pathobiologic mechanism.

We observed distinctive ^{18}F-FDG PET findings in patients with active KSHV-MCD. The most characteristic were symmetric, widespread, moderately hypermetabolic lymphadenopathy, increased splenic metabolism with splenomegaly, and, less commonly, increased marrow or salivary gland metabolism. These abnormalities resolved or improved at clinical remission. The intensity of nodal metabolic uptake during activity was correlated with symptom severity and with laboratory correlates of disease but not with HIV viremia. These findings extend those of previous case studies and retrospective series [35–38], providing more detailed evaluation of a larger cohort and, for the first time, paired comparisons of individual patients and exploration of the relationship of imaging abnormalities and clinical and laboratory correlates of disease.

The observed nodal, splenic, and marrow changes are consistent with known sites of KSHV-MCD involvement [1, 2, 42]. The findings in salivary glands are intriguing, because salivary glands are a known site of KSHV replication [43, 44], but their involvement in KSHV-MCD is unclear. The widespread abnormalities seen here provide evidence that the pathobiologic mechanism of active KSHV-MCD is generalized across nodes and spleen. We hypothesize that this reflects B-lymphocyte activation and tissue inflammation accompanying KSHV lytic activity and associated cytokine production [9–11, 45]. Moreover, this finding suggests that in KSHV-MCD, the pathologic process in individual lymph nodes is coordinated and potentiated through systemic factors. These include hIL-6, interleukin 10, and vIL-6, the last of which is produced by some KSHV-infected plasmablasts in affected lymph nodes [9]. Additional studies are needed to explore the relationship between local and systemic factors.

The ^{18}F-FDG PET abnormalities in this series were present even in subjects with suppressed HIV viral load and active KSHV-MCD. Previous studies have shown that HIV-infected patients with suppressed HIV loads do not exhibit significant ^{18}F-FDG PET abnormalities [20, 25–29]. Taken together, these data suggest that the presence of nodal and splenic ^{18}F-FDG PET abnormalities in patients with inflammatory symptoms and suppressed HIV viral load should not be simply attributed to HIV infection but should rather prompt consideration of KSHV-MCD or other diseases. Our ability to explore

the contribution of HIV viremia to ^{18}F-FDG PET abnormalities in the present study was limited by the relatively few patients with unsuppressed HIV viral load, and relatively low degree of viremia in those unsuppressed patients.

Symmetric nodal abnormalities similar in intensity to those seen here have been described in patients with high HIV viral load without KSHV-MCD. In patients without suppressed HIV load, distinguishing HIV-related reactive adenopathy from other diseases, including KSHV-MCD and lymphoma, is therefore more complex, and further studies will be required to determine the optimal imaging approach, perhaps including novel tracers [20]. Notably, extranodal abnormalities seem uncommon in these patients [27, 30], and their presence may provide a useful point of distinction.

By allowing us to characterize the range of abnormalities commonly seen in active KSHV-MCD, this series provides important information to assist physicians in distinguishing KSHV-MCD from concurrent conditions. We did not observe asymmetric or highly avid adenopathy (nodal SUV, ≥10) in any patients with KSHV-MCD alone, indicating that such changes are not characteristic of uncomplicated KSHV-MCD. This suggests that ^{18}F-FDG PET abnormalities of KSHV-MCD are distinct from those reported for high-grade lymphoma [18, 20, 22, 24] and common opportunistic infections [46], indicating that lymphoma or other diseases should be considered in patients with suspected KSHV-MCD who manifest highly avid or asymmetric adenopathy. Although ^{18}F-FDG PET is unlikely to provide a specific diagnosis, targeting biopsies for histopathology and culture to highly avid sites may improve diagnostic accuracy, minimizing sampling errors and missed diagnoses [4, 5].

These data also suggest that ^{18}F-FDG PET warrants further exploration in monitoring therapeutic response within clinical studies. The optimal approach to patient monitoring and the end point of therapy for KSHV-MCD are not defined [3, 12–14]. Resolution of ^{18}F-FDG PET abnormalities may provide useful adjunctive information supporting the decision to cease therapy. The significance of persistent minor ^{18}F-FDG PET abnormalities in otherwise well patients after therapy is uncertain and will require further assessment. Importantly, remission in this study was defined based on clinical and biochemical parameters, and the mild nodal and splenic abnormalities observed here during remission may sometimes represent persistent subclinical disease activity or immune reconstitution after completion of cytotoxic therapy. The clinical importance of these changes, along with any utility of continuing therapy beyond symptomatic remission until imaging abnormalities resolve, requires further exploration. Similarly, further study will be needed to determine whether ^{18}F-FDG PET changes are sufficiently dynamic to support interim imaging to identify patients who are not responding to therapy.

Our observations that ^{18}F-FDG PET abnormalities were present even in patients with asymptomatic disease activity and were progressive in 1 patient before relapse also suggest a role for ^{18}F-FDG PET in detecting subclinical disease. The symptoms of KSHV-MCD may develop very quickly and be life threatening [1, 3, 4], and strategies are needed to identify impending relapse. Given the observation that KSHV load increases in peripheral blood before symptomatic relapse [47], a strategy such as targeted ^{18}F-FDG PET imaging in patients with rising KSHV load may have clinical utility. Again, further studies will be required to explore this issue.

Finally, while this study was not specifically designed to assess other KSHV-associated tumors, these were present in a number of patients. In patients who also had PEL, hypermetabolic abnormalities at sites of cavitary and extracavitary PEL were delineated. Moreover, in a majority of patients who had cutaneous KS within the imaging field, the KS lesions were visualized; those where KS was not visualized included some with small lesions below scanner resolution. Because ^{18}F-FDG PET is readily available, this may be clinically useful and could complement research development of novel imaging modalities [48, 49]. Similarly, ^{18}F-FDG PET may help delineate the pathogenesis of the expanding spectrum of KSHV associated diseases, including the KSHV inflammatory cytokine syndrome [5, 50] and KS-associated immune reconstitution syndrome [51]. Its potential utility in KSHV inflammatory cytokine syndrome is being explored prospectively (NCT01419561).

Notes

References

1. Oksenhendler E, Duarte M, Soulier J, et al. Multicentric Castleman's disease in HIV infection: a clinical and pathological study of 20 patients. AIDS **1996**; 10:61.

2. Bower M, Newsom-Davis T, Naresh K, et al. Clinical features and outcome in HIV-associated multicentric Castleman's disease. J Clin Oncol **2011**; 29:2481–6.

3. Bower M. How I treat HIV-associated multicentric Castleman's disease. Blood **2010**; 116:4415–21.

4. Uldrick TS, Polizzotto MN, Yarchoan R. Recent advances in Kaposi sarcoma herpesvirus-associated multicentric Castleman disease. Curr Opin Oncol **2012**; 24:495–505.

5. Polizzotto MN, Uldrick TS, Hu D, Yarchoan R. Clinical manifestations of Kaposi sarcoma herpesvirus lytic activation: multicentric Castleman disease (KSHV-MCD) and the KSHV inflammatory cytokine syndrome. Front Microbiol **2012**; 3:73.

6. Chang Y, Cesarman E, Pessin MS, et al. Identification of herpesvirus-like DNA sequences in AIDS-associated Kaposi's sarcoma. Science **1994**; 266:1865–9.

7. Soulier J, Grollet L, Oksenhendler E, et al. Kaposi's sarcoma-associated herpesvirus-like DNA sequences in multicentric Castleman's disease. Blood **1995**; 86:1276–80.

8. Dossier A, Meignin V, Fieschi C, Boutboul D, Oksenhendler E, Galicier L. Human herpesvirus 8-related Castleman disease in the absence of HIV infection. Clin Infect Dis **2013**; 56:833–42.

9. Polizzotto MN, Uldrick TS, Wang V, et al. Human and viral interleukin-6 and other cytokines in Kaposi sarcoma herpesvirus-associated multicentric Castleman disease. Blood **2013**; 122:4189–98.

10. Aoki Y, Tosato G, Fonville TW, Pittaluga S. Serum viral interleukin-6 in AIDS-related multicentric Castleman disease. Thromb Haemost **1995**; 74:449–53.

11. Oksenhendler E, Carcelain G, Aoki Y, et al. High levels of human herpesvirus 8 viral load, human interleukin-6, interleukin-10, and C reactive protein correlate with exacerbation of multicentric Castleman disease in HIV-infected patients. Blood **2000**; 96:2069.

12. Uldrick TS, Polizzotto MN, Aleman K, et al. High-dose zidovudine plus valganciclovir for Kaposi sarcoma herpesvirus-associated multicentric Castleman disease: a pilot study of virus-activated cytotoxic therapy. Blood **2011**; 117:6977–86.

13. Gérard L, Bérezné A, Galicier L, et al. Prospective study of rituximab in chemotherapy-dependent human immunodeficiency virus associated multicentric Castleman's disease: ANRS 117 CastlemaB Trial. J Clin Oncol **2007**; 25:3350–6.

14. Hoffmann C, Schmid H, Müller M, et al. Improved outcome with rituximab in patients with HIV-associated multicentric Castleman disease. Blood **2011**; 118:3499–503.

15. Cesarman E, Chang Y, Moore PS, Said JW, Knowles DM. Kaposi's sarcoma-associated herpesvirus-like DNA sequences in AIDS-related body-cavity-based lymphomas. N Engl J Med **1995**; 332:1186–91.

16. Naresh KN, Rice AJ, Bower M. Lymph nodes involved by multicentric Castleman disease among HIV-positive individuals are often involved by Kaposi sarcoma. Am J Surg Pathol **2008**; 32:1006–12.

17. Oksenhendler E, Boulanger E, Galicier L, et al. High incidence of Kaposi sarcoma-associated herpesvirus-related non-Hodgkin lymphoma in patients with HIV infection and multicentric Castleman disease. Blood **2002**; 99:2331.

18. Seam P, Juweid ME, Cheson BD. The role of FDG-PET scans in patients with lymphoma. Blood **2007**; 110:3507–16.

19. Juweid ME, Stroobants S, Hoekstra OS, et al. Use of positron emission tomography for response assessment of lymphoma: consensus of the Imaging Subcommittee of International Harmonization Project in Lymphoma. J Clin Oncol **2007**; 25:571–8.

20. Mhlanga JC, Durand D, Tsai HL, et al. Differentiation of HIV-associated lymphoma from HIV-associated reactive adenopathy using quantitative FDG PET. Eur J Nucl Med Mol Imaging **2014**; 41:596–604.

21. Okosun J, Warbey V, Shaw K, et al. Interim fluoro-2-deoxy-D-glucose-PET predicts response and progression-free survival in patients with Hodgkin lymphoma and HIV infection. AIDS **2012**; 26:861–5.

22. Elstrom R, Guan L, Baker G, et al. Utility of FDG-PET scanning in lymphoma by WHO classification. Blood **2003**; 101:3875–6.

23. Just PA, Fieschi C, Baillet G, Galicier L, Oksenhendler E, Moretti JL. 18F-fluorodeoxyglucose positron emission tomography/computed tomography in AIDS-related Burkitt lymphoma. AIDS Patient Care STDS **2008**; 22:695–700.

24. Dunleavy K, Little RF, Pittaluga S, et al. The role of tumor histogenesis, FDG-PET, and short-course EPOCH with dose-dense rituximab (SC-EPOCH-RR) in HIV-associated diffuse large B-cell lymphoma. Blood **2010**; 115:3017–24.

25. Brust D, Polis M, Davey R, et al. Fluorodeoxyglucose imaging in healthy subjects with HIV infection: impact of disease stage and therapy on pattern of nodal activation. AIDS **2006**; 20:985–93.

26. Martin C, Castaigne C, Tondeur M, Flamen P, De Wit S. Role and interpretation of fluorodeoxyglucose-positron emission tomography/computed tomography in HIV-infected patients with fever of unknown origin: a prospective study. HIV Med **2013**; 14:455–62.

27. Sathekge M, Goethals I, Maes A, van de Wiele C. Positron emission tomography in patients suffering from HIV-1 infection. Eur J Nucl Med Mol Imaging **2009**; 36:1176–84.

28. Iyengar S, Chin B, Margolick JB, Sabundayo BP, Schwartz DH. Anatomical loci of HIV-associated immune activation and association with viraemia. Lancet **2003**; 362:945–50.

29. Scharko AM, Perlman SB, Pyzalski RW, Graziano FM, Sosman J, Pauza CD. Whole-body positron emission tomography in patients with HIV-1 infection. Lancet **2003**; 362:959–61.

30. Love C, Tomas MB, Tronco GG, Palestro CJ. FDG PET of infection and inflammation. Radiographics **2005**; 25:1357–68.

31. Bleeker-Rovers CP, de Kleijn EM, Corstens FH, van der Meer JW, Oyen WJ. Clinical value of FDG PET in patients with fever of unknown origin and patients suspected of focal infection or inflammation. Eur J Nucl Med Mol Imaging **2004**; 31:29–37.

32. Mochizuki T, Tsukamoto E, Kuge Y, et al. FDG uptake and glucose transporter subtype expressions in experimental tumor and inflammation models. J Nucl Med **2001**; 42:1551–5.

33. Gamelli RL, Liu H, He LK, Hofmann CA. Augmentations of glucose uptake and glucose transporter-1 in macrophages following thermal injury and sepsis in mice. J Leukoc Biol **1996**; 59:639–47.

34. Kubota R, Yamada S, Kubota K, Ishiwata K, Tamahashi N, Ido T. Intratumoral distribution of fluorine-18-fluorodeoxyglucose in vivo: high accumulation in macrophages and granulation tissues studied by microautoradiography. J Nucl Med **1992**; 33:1972–80.

35. Hillier JC, Shaw P, Miller RF, et al. Imaging features of multicentric Castleman's disease in HIV infection. Clin Radiol **2004**; 59:596–601.

36. Barker R, Kazmi F, Stebbing J, et al. FDG-PET/CT imaging in the management of HIV-associated multicentric Castleman's disease. Eur J Nucl Med Mol Imaging **2009**; 36:648–52.

37. Madan R, Chen JH, Trotman-Dickenson B, Jacobson F, Hunsaker A. The spectrum of Castleman's disease: mimics, radiologic pathologic correlation and role of imaging in patient management. Eur J Radiol **2012**; 81:123–31.

38. Lee ES, Paeng JC, Park CM, et al. Metabolic characteristics of Castleman disease on 18F-FDG PET in relation to clinical implication. Clin Nucl Med **2013**; 38:339–42.

39. Uldrick TS, Polizzotto MN, Aleman KA, et al. Rituximab plus liposomal doxorubicin in HIV-infected patients with KSHV-associated multicentric Castleman disease. Blood **2014**; 124:3544–52.

40. National Cancer Institute. NCI common toxicity criteria for adverse Events v3.0. Bethesda, MD: US Department of Health and Human Services, **2006**.

41. Soret M, Bacharach SL, Buvat I. Partial-volume effect in PET tumor imaging. J Nucl Med **2007**; 48:932–45.

42. Venkataraman G, Uldrick TS, Aleman K, et al. Bone marrow findings in HIV-positive patients with Kaposi sarcoma herpesvirus-associated multicentric Castleman disease. Am J Clin Pathol **2013**; 139:651–61.

43. Koelle DM, Huang ML, Chandran B, Vieira J, Piepkorn M, Corey L. Frequent detection of Kaposi's sarcoma-associated herpesvirus (human herpesvirus 8) DNA in saliva of human immunodeficiency virus-infected men: clinical and immunologic correlates. J Infect Dis **1997**; 176:94–102.

44. Bagni R, Whitby D. Kaposi's sarcoma-associated herpesvirus transmission and primary infection. Curr Opin HIV AIDS **2009**; 4:22–6.

45. Bower M, Veraitch O, Szydlo R, et al. Cytokine changes during rituximab therapy in HIV-associated multicentric Castleman disease. Blood **2009**; 113:4521–4.

46. Sathekge M, Maes A, Kgomo M, Pottel H, Stolz A, Van De Wiele C. FDG uptake in lymph-nodes of HIV+ and tuberculosis patients: implications for cancer staging. J Nucl Med Mol Imaging **2010**; 54:698–703.

47. Stebbing J, Adams C, Sanitt A, et al. Plasma HHV8 DNA predicts relapse in individuals with HIV-associated multicentric Castleman disease. Blood **2011**; 118:271–5.

48. Kainerstorfer JM, Polizzotto MN, Uldrick TS, et al. Evaluation of non-invasive multispectral imaging as a tool for measuring the effect of systemic therapy in Kaposi sarcoma. PLoS One **2013**; 8:e83887.

49. Fu DX, Tanhehco YC, Chen J, et al. Virus-associated tumor imaging by induction of viral gene expression. Clin Cancer Res **2007**; 13:1453–8.

50. Uldrick TS, Wang V, O'Mahony D, et al. An interleukin-6-related systemic inflammatory syndrome in patients co-infected with Kaposi sarcoma-associated herpesvirus and HIV but without multicentric Castleman disease. Clin Infect Dis **2010**; 51:350–8.

51. Letang E, Lewis JJ, Bower M, et al. Immune reconstitution inflammatory syndrome associated with Kaposi sarcoma. AIDS **2013**; 27:1603–13.